IEEE Access
Multidisciplinary | Rapid Review | Open Access Journal

Received June 20, 2021, accepted August 17, 2021, date of publication August 20, 2021, date of current version August 30, 2021.

Digital Object Identifier 10.1109/ACCESS.2021.3106261

Research on Wiener Degradation Model and Failure Mechanism of Interconnect Solder Joints Under Random Vibration Load

JIAYAN DONG[1], YINGLI LONG[2], XIAOXUAN JIAO[1], AND YIFENG HUANG[1]

[1]Department of Flight Control and Electrical Engineering, College of Aeronautical Engineering, Air Force Engineering University, Xi'an, Baqiao 710038, China
[2]Weihai Technician College, Weihai, Rongcheng 264300, China

Corresponding author: Jiayan Dong (machine_article@163.com)

This work was supported by the Thirteenth Five-Year Equipment Research Foundation of China under Grant 41402010102.

ABSTRACT Electronic packaging solder joints are the key parts of mechanical fixation and electrical interconnection between electronic chips and printed circuit boards, which are prone to failure and lead to electronic device failures under the action of vibration environment stress. In regard to the failure characterization and degradation modeling of electronic packaging solder joints under vibration load, this paper adopts environmental stress tests, builds a vibration failure test platform, designs a vibration load excitation spectrum, and obtains solder joint degradation data under vibration stress; it uses the square root amplitude, form factors, and kurtosis factors to characterize the solder joint degradation process, which effectively identify the solder joint degradation node, and improve the data monotonicity of the solder joint degradation process; the Wiener process is used to build a solder joint multi-stage degradation model. Based on the EM algorithm, the hyperparameters of the degradation model have been optimized, and the universal test of the Wiener degradation model with multiple samples is carried out in accordance with the LB index. The analysis shows that the effectiveness of different samples is as high as 87.5%, which verifies the universality of the Wiener degradation model; Based on the crack morphology subject to the solder joint test and the features of the solder joint in the multi-stages, the paper analyzes the crack propagation behavior of the solder joint, and clarifies the failure mechanism of the solder joint.

INDEX TERMS Solder joints, vibration stress, state characterization, degradation modeling, Wiener process.

I. INTRODUCTION

With the continuous expansion and extension of battlefield boundaries in the information age, various types of combat units, mainly aircraft, radar, reactance, and communications, have more diverse functional configurations and complex equipment components. As the main carrier of equipment function integration, electronic equipment has a broader role and a more prominent position. As the core component supporting the realization of the functions of electronic equipment, electronic packaging chips feature diverse types, dense distribution, and large numbers. Besides, due to the combat missions, equipment installations face the needs of forwarding support, long-distance maneuvering, and cross-regional garrison, which are normally exposed to harsh environments including vibration and shock, high and low temperatures, high salt and humidity, and are prone to fault and failure. Studies have shown that 70% of electronic device faults are caused by electronic packaging failures [1]–[4], while the damage in the electronic chip connection structure is the main cause of electronic packaging failures. Solder joints are a typical electronic chip connection structure, and solder joint failure has become one of the key issues that restrict the reliability of electronic equipment. Statistics show that vibration accounts for 20% of the environmental factors affecting the reliability of airborne electronic equipment [5], [6], and is the main environmental stress that causes solder joint failure. The solder joints are small, concealed in packaging, and few studies focus on the acquisition of solder joint state monitoring data and the representation of health status, while fewer systematic researches focus on the construction of degradation process models.

The researches on the characterization and degradation modeling of solder joint health under vibration load mainly

The associate editor coordinating the review of this manuscript and approving it for publication was Giambattista Gruosso.

adopt environmental stress tests and numerical simulation. Since the environmental stress test can directly obtain the state monitoring signal reflecting the failure process of the solder joint, it is more helpful to study the failure characterization and degradation modeling of the solder joint [7], [8]. This paper also uses the environmental stress test to study the solder joint failure characterization and degradation modeling. In previous studies, Kwon and Yoon [9] proposed an impedance analysis for detecting the failure of solder joints. The study pointed out that the resistance signal will change suddenly before and after the damage of the solder joint occurs, but it is difficult to characterize the gradual process of degradation. The test shows that due to crack growth, the impedance continues to increase with the deterioration of the solder joint, which can reflect the initial failure stage of the solder joint. Che and Pang [10] studied the failure behavior of QFP solder joints under vibration stress, using a high-speed camera to capture the dynamic displacement of the PCB board encapsulating the QFP chip, and regarding the displacement change as a state monitoring signal to study the characterization of solder joint failure and failure modes. Kim and Hwang [11] studied the reliability of PBGA solder joints under random vibration load. In the vibration test, the chip was encapsulated on a daisy chain circuit board to collect the solder joint electrical signals, and the solder joint resistance signal was regarded as the damage state evaluation index. The results show that the crack propagation length is closely related to the solder joint resistance. Tang *et al.* [12]–[14] realized the multi-stage degradation characterization of QFP solder joints under vibration load based on the resistance signal monitored by the experiment and divided the solder joint failure stages into a healthy state, mild failure, moderate failure and invalidate. Xu *et al.* [15] studied the life prediction method of PBGA solder joints under random vibration loads. By laying a daisy chain circuit on the PCB board to monitor the resistance of the solder joints, the health status of the solder joints can be identified and failure judgments can be made, which verifies the validity of the method. Zhang *et al.* [16] conducted a study on the failure of solder joints under random vibration load. In the experiment, a strain gauge was attached to the PCB board, and a daisy chain circuit was designed to monitor the solder joint resistance. The strain gauge senses the strain value of the PCB board near the solder joint during the vibration and the resistance value is used as a criterion for the failure of the solder joint. The results show that with the reciprocating vibration of the PCB board, the strain value also presents the characteristics of alternating changes, and when the solder joint fracture mode changes, its resistance value will increase significantly.

From the perspective of mechanical response, both electrical and strain signals can demonstrate the state changes of solder joints under environmental stress. From the perspective of failure characterization, impedance signals can directly reflect the influence of changes in the internal structure of solder joints on circuit continuity, which is more favorable compared to strain signals. As a monitoring parameter that reflects the connection status of the solder joint, the electrical signal not only reveals the moment when the solder joint fails but more importantly, it shows the process of the solder joint changing from the intact state to complete failure. Since the degradation mechanism of solder joints under vibration load is still unclear, the degradation data is highly random, and the degradation model is suitable to be constructed by a stochastic process including Wiener process, Gamma process, and Poisson process, etc., which are respectively suitable for non-strictly regular degradation processes, strictly regular degradation processes, and cumulative damage caused by shocks [17]–[19]. Cai *et al.* [20] used the Wiener process to describe the nonlinear degradation process. Liu *et al.* [21] used the stochastic Wiener process to describe the life cycle of aeroengines. Wei and Chen [22] used a multi-stage Wiener process to construct a product degradation model. This paper adopts the Wiener process to construct the solder joint degradation model under vibration load.

The paper focusing on the failure characterization and degradation modeling of solder joints under vibration load, is divided into three parts. In the first part, the paper uses the environmental tests and designs solder joint health monitoring circuits, which obtain electrical signals of solder joint status; the second part includes the multi-dimensional degradation characteristics of solder joints, the construction of a stochastic Wiener process model of solder joints, and testing the adaptability of the model with multi-sample degradation data; in the last part, the paper studies the failure mechanism of solder joints based on the multi-stage degradation statistical characteristics and the microscopic crack morphology of the solder joints.

II. VIBRATION FAILURE TEST OF SOLDER JOINTS IN ELECTRONIC PACKAGING

A. BUILDING A VIBRATION FAILURE TEST PLATFORM

Vibration failure test is an important approach to study the degradation process and failure mechanism of solder joints in electronic packaging. However, due to the small size of the solder joints and the hidden packaging location, the test firstly needs to solve the key issues of platform construction, the design of test pieces and the monitoring of parameters. This paper takes GJB150.16A and MIL-810B standards as references, and builds a vibration failure test platform as a vibration environment for solder joint failure based to the requirements of electronic packaging solder joint environmental test [23], as shown in Figure 1. The platform includes vibration test pieces, fixtures and signal monitoring devices, covering the processes of ''vibration load application'', ''vibration load transmission'', ''vibration load monitoring'', etc., and can ensure the accelerated testing of circuit board components under multi-directional complex vibration stress. To ensure that the vibration stress acts on the test pieces, the test adopts a closed-loop control system in which the vibration signal excitation is applied through the server, and the control signal is transmitted to the vibration table

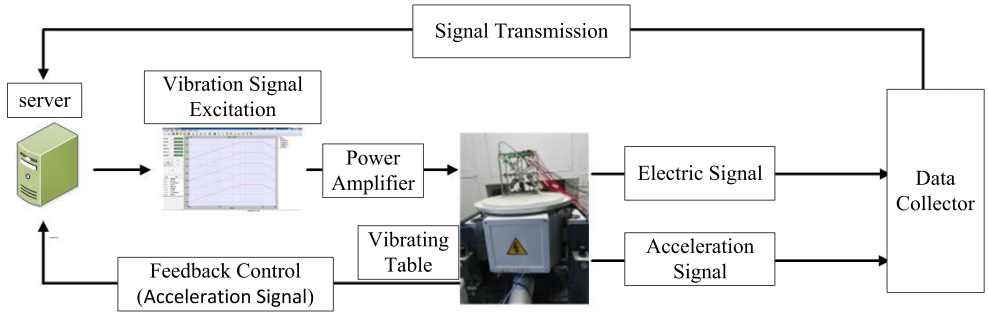

FIGURE 1. Experimental design.

through the power amplifier. The fixture acceleration is used as the loop negative feedback signal, which reacts to the excitation output of the vibration table to ensure that the test piece is in the vibration stress environment set before.

The test piece design of solder joint in electronic packaging is shown in Figure 2. The circuit board is a rectangular PCB with the length, width, and thickness of 180mm × 90mm × 0.7mm, marked as the PCB-A. A square PCB board with the size of 20mm × 20mm × 0.7mm is used as the substrate, marked as PCB-B. The solder joints are packaged between the two copper pads PCB-A board and PCB-B board, stably supporting the PCB board to prevent the direction of the stress applied by the two PCB boards to the solder joints from the deviation due to non-parallelism. In addition, the holes on the PCB provide a wire interface for the monitoring of the electrical signals of the solder joints.

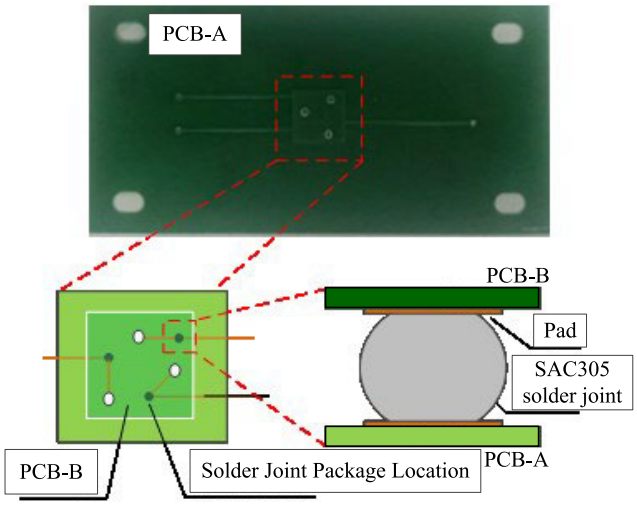

FIGURE 2. Solder joint package drawing.

The electrical signal monitoring of the solder joint is shown in Figure 3. The solder joint is packaged between the PCB-A board and the PCB-B board, and the voltage monitoring points connect the two PCB boards through the holes. The voltages that have been tested are respectively marked as U_{r1},

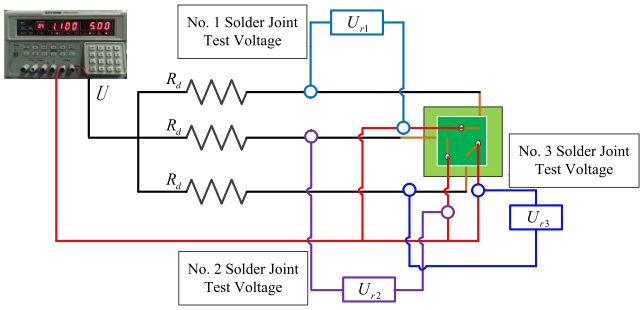

FIGURE 3. Monitoring circuit of electric signals.

U_{r2} and U_{r3}, as in

$$U_{ri} = U \times R_i / (R_i + R_d) \tag{1}$$

Among them, U is the DC power supply of the voltage divider circuit, R_d is the voltage divider resistance of the circuit, and R_i is the solder joint resistance of the branch circuit.

The DC power supply voltage is 5V. When the solder joint is intact, the resistance of the solder joint is close to 0, and the partial voltage is also approximately 0V; when the solder joint is gradually damaged, the conductive area of the test pieces of the solder joint decreases and the resistance gradually increases; when the solder joint fails, the resistance is theoretically close to infinity and the voltage tends to 5V. Therefore, the voltage amplitude of the solder joint changes from 0 to 5V from the initial state to the final failure.

B. RANDOM VIBRATION LOAD DESIGN

Due to the different operations of the equipment, the vibration stress environment of the equipment is different, in which the service environment of airborne equipment is the most severe. Therefore, this paper takes the vibration environment of jet aircraft instrumentation equipment as a reference to determine its vibration load and apply it to the failure test of solder joints. Vibration sources of airborne instrumentation equipment mainly include engine noise, airflow disturbances outside the aircraft, and structural vibration caused by aircraft maneuvering. It requires a large number of and complicated actual measurements to obtain the

actual vibration environment of the instrumentation equipment, so this paper selects the vibration spectrum type of the instrumentation equipment provided by the GJB150.16A as a reference to determine the test load. The random power spectrum density [24]–[26] is shown in Figure 4.

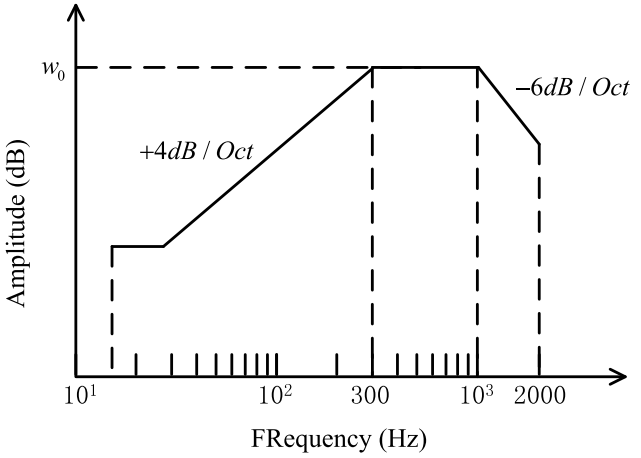

FIGURE 4. Vibration environment of jet aircraft dashboard.

Figure 4 shows that the up and down slopes of the random power spectral density and the frequency range have been determined. The parameters to be determined in the test are the initial frequency and the acceleration power spectral density value W_0 (unit: g2/Hz), and the values are 0.01, 0.02, 0.03, 0.04, 0.05, 0.06 and the frequency is relatively high. This paper uses $W_0 = 0.03g^2/Hz$ to design the acceleration power spectrum and conduct experiments, in which the random vibration load design is shown in Figure 5.

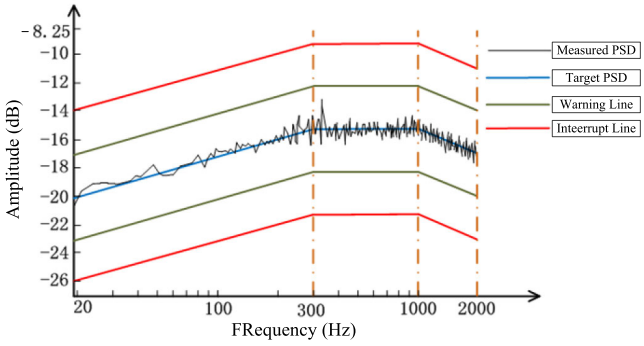

FIGURE 5. Random vibration power spectrum.

The PSD value ±3dB sets the alarm line and ±6dB sets the interrupt line. When the vibration parameters in the test are abnormal, there will be a warning until the test is interrupted by itself to ensure that the vibration parameters are controlled within the specified value ±3dB during the entire test process. By comparing the input and output PSD curves, the excitation signal is nearly consistent with the measured signal, which does not have large peaks, indicating that the fixture design features good transfer and also ensures the successful failure test of the solder joint under specific stress.

III. CHARACTERIZATION OF SOLDER JOINT HEALTH STATUS

This paper uses environmental stress testing to obtain the data in the solder joint degradation process, as shown in Figure 6. The voltage amplitude of the solder joint does not change significantly at first, and then the peak value is close to 0.5V, and finally increased sharply and quickly reaching a failure state. Under the vibration stress, cracks in the solder joints gradually sprout, and the opening and closing of the cracks lead to the repeated changes in the effective energized area of the solder joints and changes in the voltage amplitude.

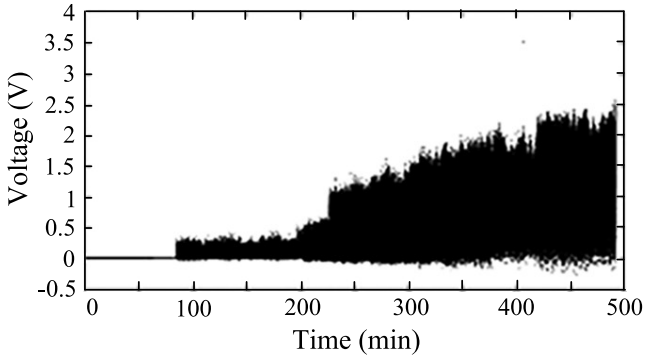

FIGURE 6. Solder joint voltage change graph.

Under the vibration stress, the solder joint cracks are in a state of periodic opening and closing during the vibration, and the solder joint voltage alternately changes between peak and valley values. At the beginning of the vibration, the solder joints are intact and no cracks are generated; with the continuous vibration stress, cracks in the solder joints begin to grow, and the accumulation of solder joint deformation reaching to a certain level may cause brittle fracture of the solder joints. During the vibration process of the solder joints, on the one hand, due to the continuous target load, the solder joints alternately bear the pressure and tension exerted by the PCB board; on the other hand, the time lag between the acceleration of the solder joint reaching to the peak and the PCB board deformation reaching the extreme value leads to the repeatedly compression and stretch of the solder joints [27], [28].

According to the electrical signal monitoring data in the solder joint degradation process, solder joint degradation is a multi-stage degradation process. However, the electrical signal reflects the change in the resistance of the solder joint, whose data curve features insignificant monotonic change, large numerical fluctuation range, and difficulty in determining the moment of phase transition, and it cannot fully characterize the change in the health state of the solder joint. For this problem, this paper selects time-domain statistics such as peak value, mean value, root square amplitude, standard deviation, variance, crest factor, and kurtosis factor to demonstrate the solder joint degradation process. The research has shown that compared with the peak value, mean value, standard deviation, and variance, the root square amplitude is

the most monotonic, and can best reflect the degradation process of solder joints, while kurtosis factor and crest factor are more sensitive to the transition moment of solder joint degradation process [29], [30]. This paper also uses the square root amplitude, form factor, and kurtosis factor to describe the solder joint degradation process under random vibration loads, as shown in Figure 7.

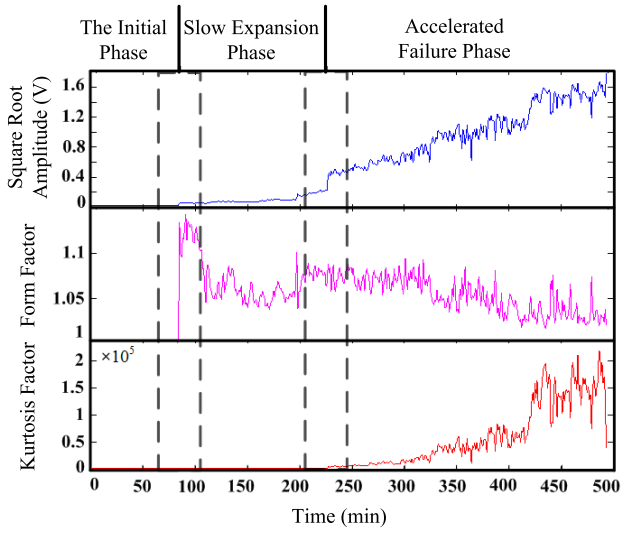

FIGURE 7. Degradation process of solder joints under random vibration load.

The figure above shows that the square root amplitude, crest factor and, kurtosis factor demonstrate the degradation characteristics of solder joints from different aspects. The root square amplitude is the most monotonic, while the crest factor and kurtosis factor are more sensitive on the failure state of solder joints. Based on the three statistics, the analysis shows that the form factor effectively identifies the first inflection point of the solder joint degradation process, and the solder joint electrical signal is distorted 87 minutes later, and the square root amplitude changes from 10^{-3} to 10^{-1}; The kurtosis factor effectively identifies the second inflection point of the solder joint degradation process, and the solder joint electrical signal enters the accelerated failure phase at 227 minutes. Therefore, the solder joint degradation process can be divided into three stages. In the first stage, the solder joints are intact and the data is stable, indicating that no cracks have initiated; in the second stage, the signal has been distorted, and the voltage root amplitude gradually increases, indicating the growth of the solder joints crack and the slow expansion; in the third stage, The signal peak and valley value greatly increase. The solder joint signal amplitude changes more drastically, and the solder joint is in the accelerated failure stage.

IV. WIENER DEGRADATION MODEL CONSTRUCTION

A. DEGENERATE EQUATION BASED ON WIENER PROCESS

According to the nature of the Wiener process, the time series difference $\{S(t), t \geq 0\}$ obeys the normal distribution, that is $S(t+\Delta t) - S(t) \sim N(\Delta t \cdot \mu, \Delta \cdot \sigma 2)$, where μ is the drift parameter of $S(t)$ and σ is the diffusion parameter of $S(t)$.

In actual situations, the time series tend to change away from the initial value, that is $\mu \neq 0$. When the parameters μ and σ in the Wiener process model are constant, there is no difference between degraded samples, that is, the difference of the same batch of solder joints can be ignored. In fact, due to uncontrollable factors, there are bound to be differences between solder joint samples. Therefore, model parameters vary with sample selection. In this regard, this paper takes μ and σ as the random variables, and the Wiener process model [31], [32] that introduces the random effect of parameter changes is expressed as $S(t) = \mu t + \sigma W(t)$, where μ and σ obey the joint distribution of normal-inverse Gamma [33]. In accordance with the random effect analysis of the Wiener process, μ and σ are both random variables. To define $G = \sigma - 2$, it can be assumed to obey the Gamma distribution, that is:

$$f(G) = (\beta^{\alpha} / \Gamma(\alpha)) \times G^{\alpha+1} \times \exp(-\beta G) \tag{2}$$

In formula (2), the Gamma distribution parameters G, α and β are all positive numbers. On this basis, it can be assumed that under the given premise G, μ obeys the normal distribution, that is $\mu|G \sim N(p, q \cdot G^{-1})$.

The Wiener process is suitable for processing linear degradation processes while actually product degradation processes are often non-linear and cover multiple degradation stages. According to the identification of the solder joint degradation process under random vibration load, each degradation stage of the solder joint can be approximately regarded as linear degradation. This paper establishes the solder joint segmentation model based on the Wiener process as in

$$X(t) = \begin{cases} \mu_0 t + \sigma_0 B(t) & t \leq T_1 \\ l_1 + \mu 1(t - T_1) + \sigma_1 B(t) & T_1 \leq t \leq T_2 \\ l_2 + \mu_2(t - T_1 - T_2) + \sigma_2 B(t) & T_2 < T_1 \end{cases} \tag{3}$$

In the formula, l_1 and l_2 respectively represent the distance between the initial value of the corresponding degradation stage and the horizontal axis, and the time T_1 and T_2 are obtained by pre-analyzing the statistic form factor and kurtosis factor.

B. OPTIMIZATION OF MODEL PARAMETERS BASED ON THE EM ALGORITHM

The acquisition of model parameters firstly needs to obtain the prior values of hyperparameters. This paper studies the iterative optimization of prior values based on the EM algorithm. The EM algorithm is easy to calculate, and the results have good convergence, which often used to solve the maximum likelihood function. Following the Bayesian formula, the posterior estimated value of the hyperparameter is obtained [34], as shown in formula (4):

$$B(\mu, G|S) = \frac{L(S|\mu, G) \cdot B(\mu, G)}{\int_0^{+\infty} \int_0^{+\infty} L(S|\mu, G) \cdot B(\mu, G) d\mu dG} \tag{4}$$

In the formula, $L(S|\mu, G)$ represents a maximum likelihood function. $B(\mu, G)$ is a priori density function, and $B(\mu, G|S)$ is a posterior density function. $L(S|\mu, G)$ and $B(\mu, G)$ are shown in formulas (5) and (6) respectively.

$$B(\mu, G) = \frac{G^{1/2}}{\sqrt{2\pi q}} e^{\frac{-G(\mu-p)^2}{2q}} \frac{\beta^\alpha G^{\alpha+1}}{\Gamma(\alpha)} e^{-\beta G} \tag{5}$$

$$L(S|\mu, G) = \prod_{i=1}^{n} \frac{G^{1/2}}{\sqrt{2\pi\,\Delta(t_i)}} e^{\frac{-G(\Delta S_i - \mu\Delta(t_i))^2}{2\Delta(t_i)}} \tag{6}$$

According to the prior and posterior density functions of drift parameters and diffusion parameters, when the hyperparameters $\alpha^*, \beta^*, p^*, q^*$ obtained, posterior iteration equations can be verified as in

$$\alpha^* = \frac{N}{2} + \alpha \tag{7}$$

$$\beta^* = \beta + \frac{p^2}{2q} - \frac{(S_n q + p)^2}{2(t^n q^2 + d)} + \sum_{i=1}^{n} \frac{\Delta S_i^2}{2\Delta t_i} \tag{8}$$

$$p^* = \frac{S_n q + p}{t_n q + 1} \tag{9}$$

$$q^* = \frac{q}{t_n q + 1} \tag{10}$$

This paper has carried out 8 batches of solder joint failure tests, so the sample data in the priori parameter estimation is the degradation process data of the 8 solder joint samples. $S_i = \{S_{1i}, S_{2i}, \ldots, S_{ni}\}$ is the degradation data of the life process of the j^{th} sample. The measurement time of t_{ij} refers to each measurement value S_{ij}. i represents the number of measurements in the process, where $i = 1, 2, \ldots, n$ and $j = 1, 2, \ldots, N(N = 8)$. The 8 samples are used as prior information to establish the likelihood function [35]–[37], as in formula (11).

$$\begin{aligned} L(\mu_j, G_j, \alpha, \beta, p, q) = &\prod_{i=1}^{n}\prod_{j=1}^{N} \frac{G_j^{0.5}}{\sqrt{2\pi\,\Delta t_{ij}}} e^{\frac{-G_j(\Delta S_{ij} - \mu_j \Delta t_{ij})^2}{2\Delta t_{ij}}} \\ &\times \prod_{j=1}^{N} \frac{G_j^{0.5}}{\sqrt{2\pi q}} e^{\frac{-w_j(\mu_j - p)^2}{2q}} \\ &\times \frac{\beta^\alpha G_j^{\alpha-1}}{\Gamma(\alpha)} e^{-\beta G_j} \end{aligned} \tag{11}$$

Formula (11) includes model parameters μ_j, G_j and hyperparameters α, β, p, q. The iterative equation of hyperparameter [38] estimates as in

$$\varphi(\hat{\alpha}) - \ln\hat{\alpha} = \frac{1}{N}\sum_{j=1}^{N} \ln G_j + \ln N - \ln \sum_{j=1}^{N} \ln G_j \tag{12}$$

$$\hat{\beta} = N \cdot \hat{\alpha} \Big/ \sum_{j=1}^{N} G_j \tag{13}$$

$$\hat{p} = \sum_{j=1}^{n} G_j \mu_j \Big/ \sum_{j=1}^{n} G_j \tag{14}$$

$$\hat{q} = \frac{1}{N}\sum_{j=1}^{n} (G_j \mu_j^2 - 2\hat{p} G_j \mu_j + \hat{p}^2 G_j \tag{15}$$

In the above formula, $\varphi(\cdot)$ refers to the diGamma function. μ_j and G_j are the undetermined variables. The hyperparameter estimates, cannot be directly calculated by the model parameters. The EM algorithm is required to obtain the expected values μ_j and G_j including $E(G_j), E(lnG_j), E(G_j\mu_j)$, and $E(G_j\mu_j^2)$, then substitute it into the iterative equation to replace μ_j and G_j. Since μ and G obey the conjugate prior distribution of normal-inverse Gamma, the iterative equation of expected value [39] can be derived as follows.

$$E(G_j) = \frac{\hat{\alpha}_j + n_j/2}{\hat{\beta}_j + \frac{\hat{p}_j^2}{2\hat{q}_j} - \frac{(\hat{q}_j s_{nj} + \hat{p}_j)^2}{2(t_{nj}\hat{q}_j^2 + \hat{q}_j)} + \sum_{i=1}^{n} \frac{\Delta s_{ij}^2}{2\Delta t_{ij}}} \tag{16}$$

$$\begin{aligned} E(\ln G_j) = &\varphi(\hat{\alpha}_j + \frac{n_j}{2}) \\ &- \ln(\hat{\beta}_j + \frac{\hat{p}_j^2}{2\hat{q}_j} - \frac{(\hat{q}_j s_{nj} + \hat{p}_j)^2}{2(t_{nj}\hat{q}_j^2 + \hat{q}_j)} + \sum_{i=1}^{n} \frac{\Delta s_{ij}^2}{2\Delta t_{ij}}) \end{aligned} \tag{17}$$

$$E(G_j\mu_j) = E(G_j E(\mu_j|G_j)) = E(G_j)\frac{\hat{q}_j s_{nj} + \hat{p}_j}{t_{nj}\hat{q}_j + 1} \tag{18}$$

$$E(G_j\mu_j^2) = E(G_j)(\frac{\hat{q}_j s_{nj} + \hat{p}_j}{t_{nj}\hat{q}_j + 1})^2 + \frac{\hat{q}_j}{t_{nj}\hat{q}_j + 1} \tag{19}$$

In the above formula, the hyperparameter estimates are the calculated values after the j^{th} iteration. On the basis of obtaining the parameters-including expectations, the $E(G_j)$, $E(lnG_j)$, $E(G_j\mu_j)$ and $E(G_j\mu_j^2)$ are substituted into the iterative formulas (12) to (15), so that the hyperparameter estimates can be obtained after $j+1$ steps. After the calculation results of the j and $j+1$ steps meet the iteration accuracy, the hyperparameter estimates of the $j+1$ step are the prior estimates.

To apply Wiener process modeling, the difference of each degradation stage of the solder joints is firstly tested with a significance level of 0.1 normality, and then a hypothesis is made:

H_0: The degraded component difference obeys the normal distribution;

H_1: The degraded component difference does not obey the normal distribution.

The paper adopts Lilliefors test, an improvement of Kolmogorov-Smirnov test, which is only applicable to test the standard normal distribution, while Lilliefors test is also applicable to the general normal test.

The Lilliefors test is as follows. For the increments of n samples, namely $\Delta S = (\Delta s_1, \Delta s_2, \ldots, \Delta s_{n-1})$, the degradation data is standardized according to the following formula.

$$z_i = \Delta s_i - \hat{\mu}/\hat{\sigma} \tag{20}$$

On this basis, according to the size order of z_i, the empirical distribution function of $F_n(z)$ is obtained from the new order of $z_{(i)}$, and then the test statistic [40] is obtained, as in

$$D_n = \sup|F_n(z) - \phi(z)| \tag{21}$$

In accordance with the critical value $D_{n1-\alpha}$ under the significance level α, when $D_n \geq D_{n1-\alpha}$, reject H_0, and the difference of degraded data is not normally distributed; when $D_n < D_{n1-\alpha}$, then accept H_0, and the difference of degraded data is normally distributed. Lilliefors normal test is used to analyze the normality of the difference of solder joint degradation under simple harmonic vibration load. At the significance level of 0.1, the accepted sample obeys the normal distribution. The normal distribution inspection curve of each stage of the solder joint is shown in Figure 8.

In the solving process of model parameters, the initial value of hyperparameters α, β, p, q are set to 0.1, 0.1, 0.1, 0.1. When the iteration accuracy of the four hyperparameters e_1, e_2, e_3 and e_4 are all less than 10^{-6}, the iteration stops, and the iterative value at this time is selected as the a priori estimated value of the hyperparameter. The calculation formula of iteration accuracy e_i is as in

$$\begin{cases} e_1 = \left|\hat{\alpha}_n - \hat{\alpha}_{n+1}\right| & e_2 = \left|\hat{\beta}_n - \hat{\beta}_{n+1}\right| \\ e_3 = \left|\hat{p}_n - \hat{p}_{n+1}\right| & e_4 = \left|\hat{q}_n - \hat{q}_{n+1}\right| \end{cases} \tag{22}$$

After the iterative calculation, the priori estimates of hyperparameter are marked as $\hat{\alpha}$, $\hat{\beta}$, $\hat{p}$, $\hat{q}$. Priori estimates are substituted into the hyperparameter posterior probability formula, which generates hyperparameter posterior estimates including α^*, β^*, p^*, q^*. The hyperparameter estimates of the three degradation stages are shown in Table 1. The solder joint degradation curve is shown in Figure 9. The degradation trajectory and degradation curve show that the degradation process of solder joints can be characterized with the construction of the degradation model based on the Wiener process.

TABLE 1. Hyperparameter estimates under random vibration load.

Hyperparameter		α	β	p	q
Phase I	Prior Estimate	1.00E-03	2.74E-11	4.00E+04	5.84E+16
	Posterior Estimate	4.20E+01	2.17E-06	2.27E-04	1.19E-02
Phase II	Prior Estimate	1.00E-03	1.28E-09	1.49E+03	1.74E+12
	Posterior Estimate	5.60E+01	4.02E-05	8.54E-04	8.93E-03
Phase III	Prior Estimate	1.00E-03	4.64E-06	2.87E+00	1.77E+03
	Posterior Estimate	1.48E+02	1.30E-03	4.95E-03	3.38E-03

The Wiener degradation model of solder joints researched and constructed in this paper can better describe the degradation process of solder joint structure. And the model is a key step in the research of solder joint remaining life prediction. After that, the model failure probability density function and failure probability distribution function can be further derived, and then the probability distribution and estimation method of the remaining life can be established. At last,

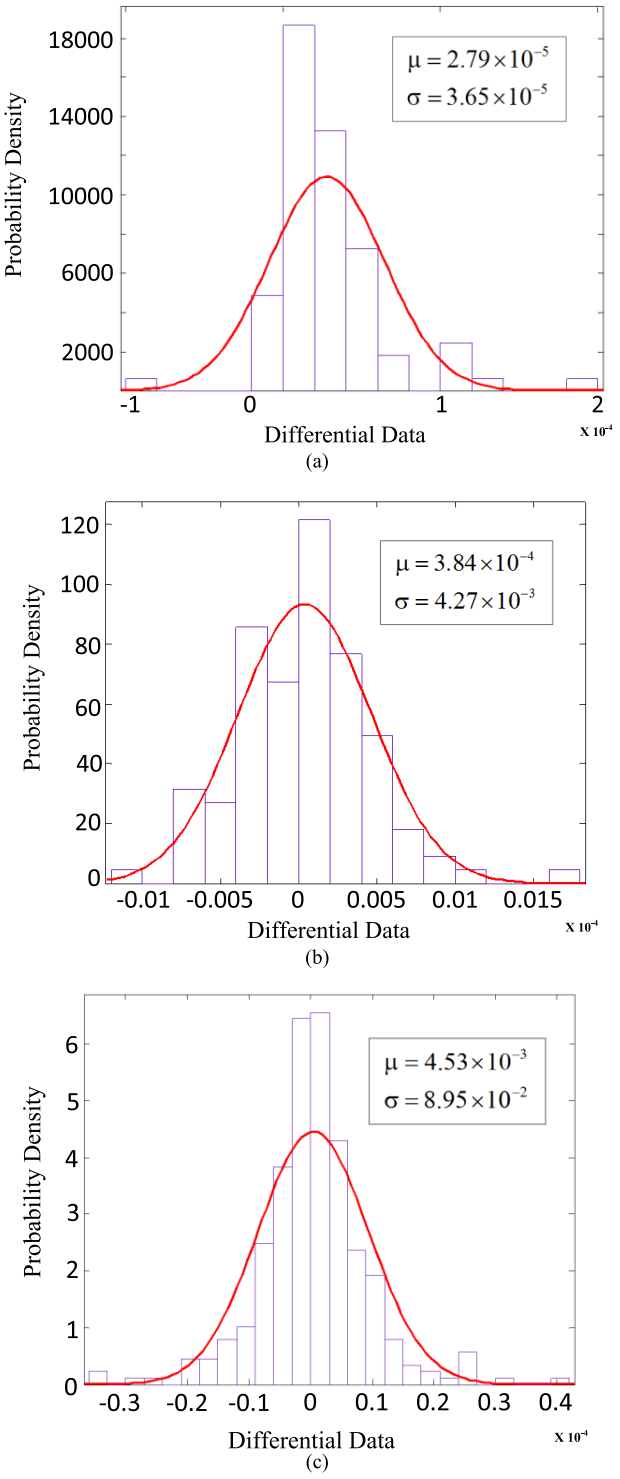

FIGURE 8. Degradation differential data distribution curve.

these model foundation can be applied to the remaining life prediction and health management research of solder joints.

C. INSPECTION OF SOLDER JOINT DEGRADATION MODEL BASED ON LB INDEX

The Wiener degradation model based on the EM algorithm takes the degradation data of a single solder joint as the

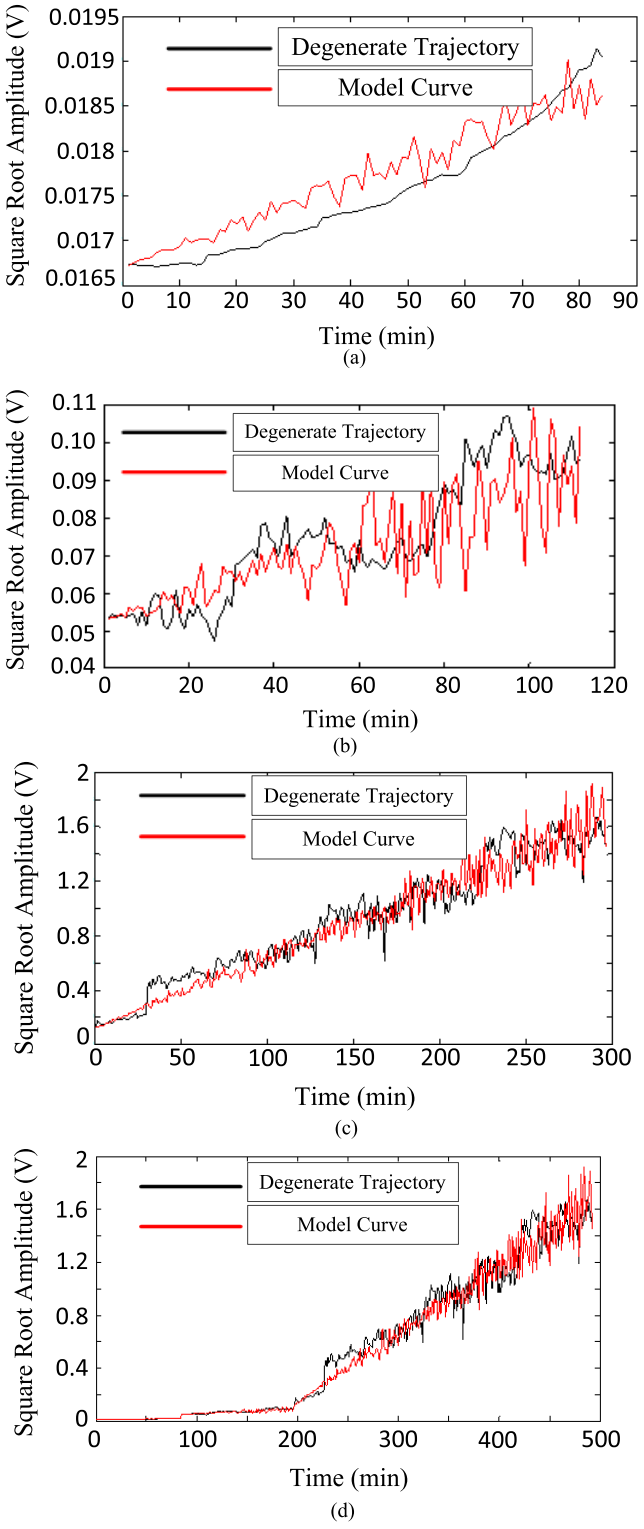

FIGURE 9. Degradation curve of solder joint under random vibration load.

modeling object. The adaptability of the model to multiple samples under the same vibration stress needs to be further inspected. This paper adopts the white noise test to verify the effectiveness of the model, that is, the white noise analysis on the residual sequence of the model is conducted with the LB (Ljung-Box) index. When the model takes the white noise significance test, it indicates that the degradation model fully shows the characteristics of the failure data, and vice. The calculation of LB index [41] as follows:

$$LB = n(n+2)\sum_{i=1}^{m}(\hat{\rho}^2(i)\Big/(n-i)) \tag{23}$$

where n is the number of samples and $\hat{\rho}^2(i)$ is the correlation coefficient of sample order delay of k. This statistic obeys the chi-square distribution and the degree of freedom is m. Given the significance level $\alpha = 0.05$, the rejection domain is LB $> \chi^2_{1-\alpha,\mathrm{m}}$. The null hypothesis and alternative hypothesis of LB test are:

$$H_0 : \hat{\rho}_1^2 = \hat{\rho}_2^2 = \cdots = \hat{\rho}_m^2;$$

H_1: At least certain $\hat{\rho}_k^2(k \le m)$ is not equal to 0.

The valid null hypothesis indicates that the sample data are independent, and the null sequence is considered as a white noise sequence; otherwise, the sample residuals are considered to be correlated, and the null sequence is not a white noise sequence.

This paper adopts the Wiener degradation model to characterize the degradation processes of multiple solder joints under the same vibration stress, and calculates the residuals based on the model results, and then the residuals are tested for significance. When the significance probability is greater than 0.05, namely, the return logic value is 0, which means that there is not enough evidence to reject the null hypothesis that the residual sequence is not autocorrelated; when the significance probability is less than 0.05, that is, the return logic value is 1, which means that the residual sequence has autocorrelation at the significance level of 0.05, and the null hypothesis is invalid. The significance probability and logical value results of each sample degradation model are shown in Table 2.

TABLE 2. White noise test result.

Sample Number	LB	Logical Value	Significance Probability
1	1.68	0	1
2	27.5	0	0.1199
3	12.0	0	0.916
4	2.73	0	1
5	3.57	0	1
6	12.2	0	0.9065
7	52.8	1	0.0001
8	4.94	0	0.9997

The white noise test results in Table 2 show that the 7 samples under random vibration load passed the white noise test with the pass rate of 87.5%, indicating that the Wiener model can fully show the information of the solder joint degradation process and can be used as a model to characterize the degradation process of solder joints.

V. ANALYSIS OF MICROSCOPIC FAILURE MECHANISM OF SOLDER JOINTS

To further analyze the microscopic failure behavior of solder joints under random vibration load, this paper selects solder joints with voltage peaks in the range of (0, 0.1), (0.1, 0.5), (0.5, 1), (1, 1.5), (1.5, 5) for electron microscope observation, and marks the solder joints as R_1, R_2, R_3, R_4 and R_5.

The voltage amplitude range of the solder joints R_1 is between 0 and 0.1. The signal amplitude and electron microscope observation results are shown in Figure 10, which show that the square root amplitude value of the statistic is about 0.026, indicating that the state of the solder joint is still in the first phase. There are cracks in the right and middle of the solder joints, and no traces of cracks in the solder joints near the Cu pad and the Cu pad area. The distribution of internal cracks in the solder joints also verifies that the solder joints are basically intact.

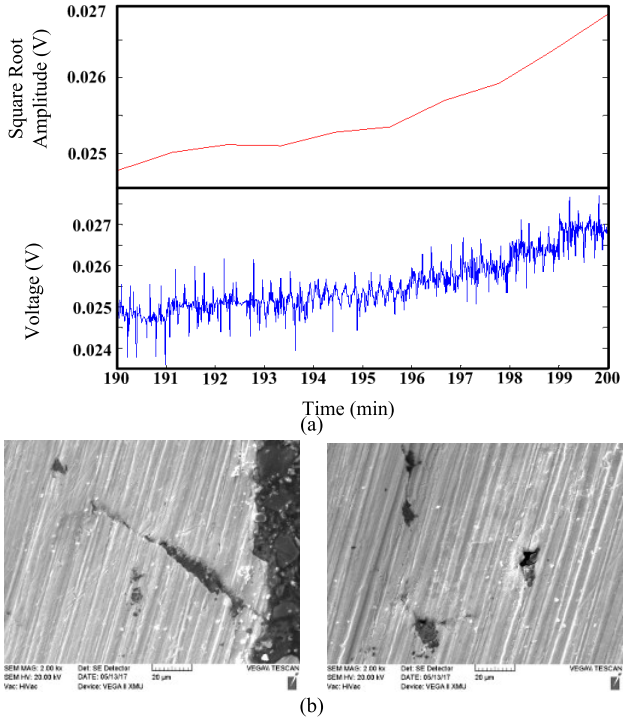

FIGURE 10. (a) Signal amplitude and (b) crack growth behavior of the first group of solder joints.

The peak voltage range of the solder joints R_2 is between 0.1 and 0.5. The signal amplitude and electron microscope observation results are shown in Figure 11. Based on the change in the amplitude of the electrical signal in Figure 11, combined with the observation and analysis of the electron microscope, it is found that the state of the solder joint has changed and entered the second stage of failure. On both sides of the solder joint, the obvious cracks appear, and the solder changes loosely with the number of cracks increases.

The peak voltage range of the solder joint R_3 is between 0.5 and 1. The signal amplitude and electron microscope

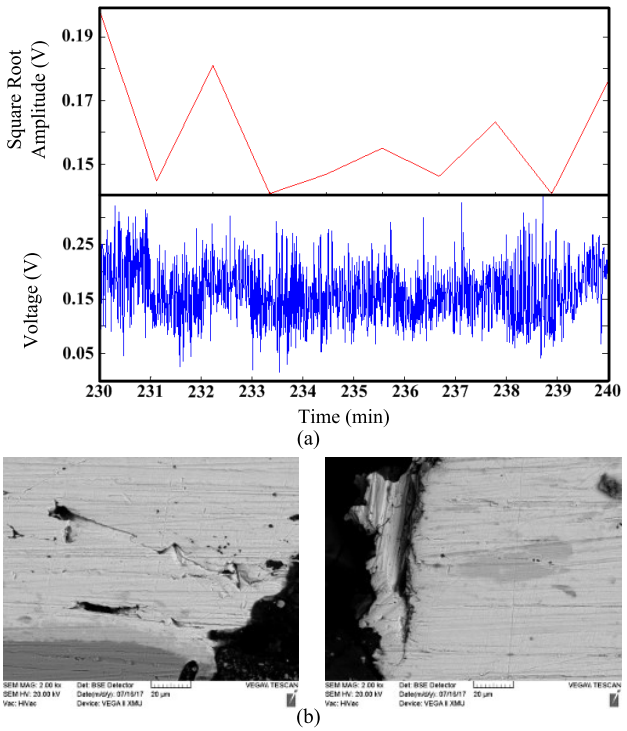

FIGURE 11. (a) Signal amplitude and (b) crack growth behavior of the second group of solder joints.

observation results are shown in Figure 12. Compared with the square root amplitude of the solder joint R_2, the signal amplitude has over doubled, and the damage of the solder joint obviously increases. The cracks of solder joint R_3 spread laterally along the inner side of the solder joint close to the copper pad. The main component of the IMC layer formed on the part of the Cu pad surface that is in contact with the Sn solder is Cu6Sn5 crystals, which is brittle and prone to breakage under stress load.

The peak voltage range of the solder joint R_4 is between 1 and 1.5. The signal amplitude and electron microscope observation results are shown in Figure 13 respectively, which shows that the amplitude of the electrical signal has increased significantly, and the damage of the solder joint cracks has also been further increased. The solder joint cracks originate in the IMC layer at the junction of the solder joint and the Cu pad and expand downward, penetrating the solder joint longitudinally.

The peak voltage range of the solder joints R_5 is between 1.5 and 5. The signal amplitude and electron microscope observation results are shown in Figure 14. The amplitude of the electrical signal in Figure 14 has exceeded 2V and stabilized at this amplitude, while the root square amplitude of the degradation is also about 1.8, indicating that the solder joint basically failed. There are multiple cracks in the solder joints R_5, among which the cracks that have the greatest impact on the solder joints originate from the outside of the solder joints, extending laterally along the Cu pads, finally

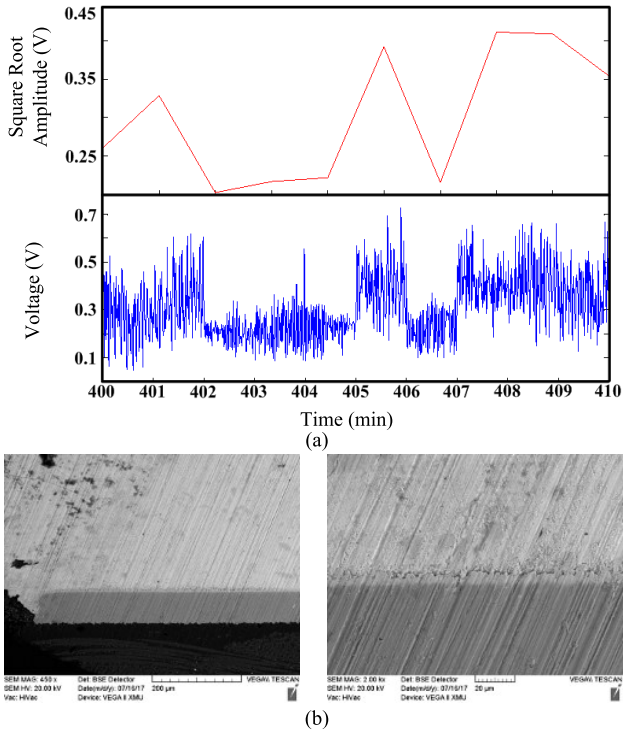

FIGURE 12. (a) Signal amplitude and (b) crack growth behavior of the third group of solder joints.

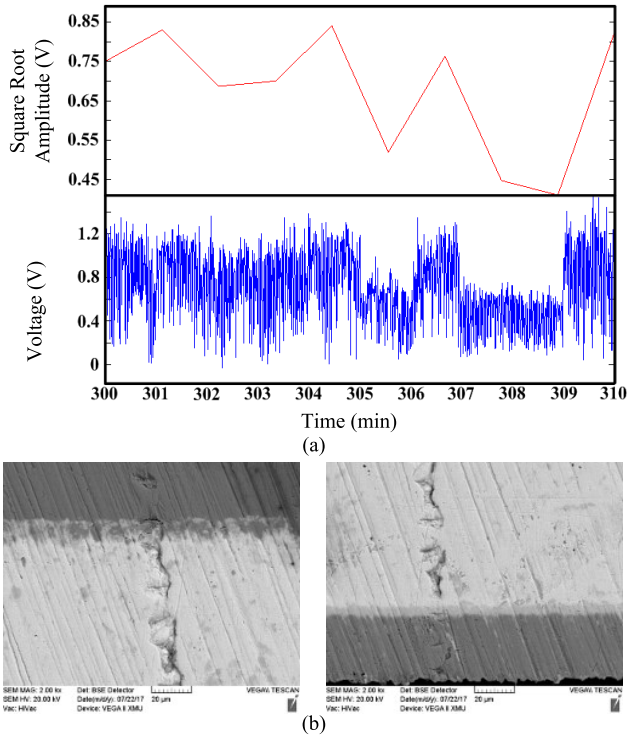

FIGURE 13. (a) Signal amplitude and (b) crack growth behavior of the fourth group of solder joints.

penetrating the Cu pads, which leads to the failure of the solder joints.

Through the analysis of the microscopic failure behavior of the solder joints, it shows that the distribution of solder

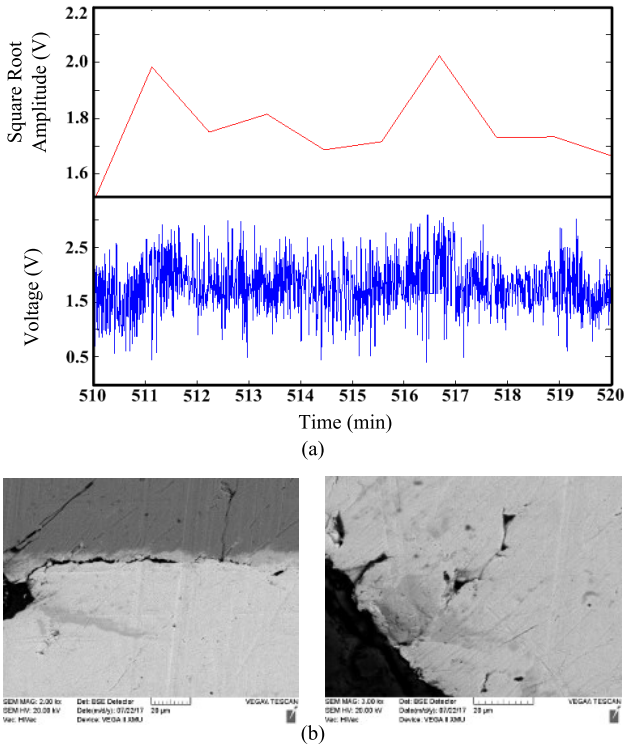

FIGURE 14. (a) Signal amplitude and (b) crack growth behavior of the fifth group of solder joints.

TABLE 3. Solder joint crack distribution statistics under the random vibration load.

Solder Joint Number	Horizontal Width /um	Total Width /um	Percentage
R_1	10.21	2333.32	11.01
R_2	15.44	2201.87	9.95
R_3	514.38	2058.35	0.74
R_4	71.43	2100.96	100.00
R_5	14.26	2245.31	100.00
Solder Joint Number	Longitudinal Length /um	Total Width /um	Percentage
R_1	103.13	936.52	0.44
R_2	84.60	850.67	0.70
R_3	5.43	735.72	24.99
R_4	564.29	564.29	3.40
R_5	65.22	65.22	0.64

joint cracks covers four positions: both sides of the solder joint, the inside of the solder joint near the cavity, between the solder joint and the Cu pad, and within the Cu pad. With the reciprocating vibration of the PCB board, the edge position of the solder joint gradually becomes loose under the action of alternating stress, which leads to the initiation and expansion of cracks. The microscopic analysis of solder joint cracks shows that the increase of solder joint damage under vibration load leads to the increase of the degradation characteristic value. To compare the damage degree of the solder joints

under different degradation levels, the statistics of the crack with the largest percentage of the horizontal and vertical width of the corresponding area in the horizontal and vertical length of each solder joint are shown in Table 3. The increase percentage of cracks of R_1-R_3 in the horizontal length is not as obvious as that in the horizontal length. The cracks of R4-R5 grow rapidly vertically. The change of solder joint cracks is similar to the solder joint monitoring signal. However, due to the uncertainty of the time threshold of the solder joint degradation stage, and the observation of the solder joint with the electron microscope are all post-observations, it is difficult to strictly match the solder joint crack growth behavior and the solder joint degradation process together. The solder joint crack and solder joint state monitoring signals are a kind of qualitative correlation, further quantitative research and error analysis require simulation and experimental observation based on a large number of experiments.

VI. CONCLUSION

This paper focuses on the health characterization and degradation modeling of solder joints under vibration loads. Based on the vibration environment of the airborne electronic equipment, firstly the solder joint vibration failure test platform is built, and the vibration load excitation spectrum, test pieces and electrical signal monitoring circuit are designed, from which the solder joint degradation data under vibration stress are obtained. On this basis, the square root amplitude, form factor, and kurtosis factor are used as the characteristics of the solder joint degradation process, which effectively identify the solder joint degradation node and improve the data monotonicity of the solder joint degradation process. For the problem of solder joint degradation modeling, the paper adopts the Wiener process to build a solder joint multi-stage degradation model. Based on the EM algorithm, the model's hyperparameter solution is optimized. The paper carries out an adaptability test on the Wiener degradation model under multiple samples based on the LB index, which verifies the universality of Wiener degradation model. Finally, based on the characteristics shown in the solder joint degradation process, and with the comprehensive solder joint metallographic analysis, the paper distinguishes the solder joint multi-stage degradation process, studies the solder joint micro crack propagation behavior, and verify the effectiveness of the solder joint health status feature expression from the micro aspect. The micro-failure mechanism of solder joints has been summarized and studied simultaneously. The paper studies the test platform, the test design, the selected health characteristics, the Wiener degradation model of the solder joints, and the microscopic failure mechanism of the solder joints obtained from the analysis, which can provide approaches and the theoretical reference for the reliability study and degradation research of the chip electronic connection structure.

Research on solder joint degradation model and failure behavior is the basis of solder joint life prediction and health management research. It is also the basis for the state assessment of electronic equipment. Due to the differences in solder joint samples and the complexity of the equipment service environment, there are also certain differences in solder joint degradation rate and degradation volatility. This paper is based on the EM algorithm to achieve the solution of the degenerate model parameters and hyperparameters. However, the analysis of model differences under different samples, the construction of physical models for solder joint failure, the prediction of the remaining life of solder joints and health management, and even the state assessment and health management research at the electronic equipment level require more in-depth research.

ACKNOWLEDGMENT

The authors would like to thank Prof. Yingli Long for her advice and guidance on the experimental design of this article, appreciate Xiaoxuan Jiao for his valuable suggestions on the article, and Prof. Yifeng Huang for his suggestions and help with the studies in the article.

REFERENCES

[1] Q. Guo, M. Zhao, and H. Wang, "SMT solder joint's semi-experimental fatigue model," *Mech. Res. Commun.*, vol. 32, no. 3, pp. 351–358, May 2005.
[2] B. Mirman, "Tools for stress analysis of microelectronic structures," *J. Electron. Packag.*, vol. 122, no. 3, pp. 280–282, Sep. 2000.
[3] J. Hu, B. Jing, Y. Huang, X. Jiao, M. Sun, and L. Li, "A health indicator for interconnect structure of QFP package under vibration and steady temperature," *IEEE Access*, vol. 8, pp. 122898–122907, 2020.
[4] X. Zhou, "Reliability analysis of board-level lead-free solder joints under drop impact load," M.S. thesis, School Mech. Eng., Shanghai Jiao Tong Univ., Shanghai, China, 2007.
[5] T. T. Mattila, J. Hokka, and M. Paulasto-Kröckel, "The reliability of microalloyed Sn-Ag-Cu solder interconnections under cyclic thermal and mechanical shock loading," *J. Electron. Mater.*, vol. 43, no. 11, pp. 4090–4102, Nov. 2014.
[6] J. X. Hu, J. Bo, and T. Wei, "Thermal effect simulation and reliability analysis of lead-free micro solder joints," *Electron. Compon. Mater.*, vol. 35, no. 3, pp. 81–84, 2016.
[7] X. Zhou, X. Lu, X. Cao, Z. Liu, and Y. Chen, "Research on life evaluation method of solder joint based on eddy current pulse thermography," *Rev. Sci. Instrum.*, vol. 90, no. 8, Aug. 2019, Art. no. 084901.
[8] M. A. Gharaibeh and J. M. Pitarresi, "Random vibration fatigue life analysis of electronic packages by analytical solutions and Taguchi method," *Microelectron. Rel.*, vol. 102, Nov. 2019, Art. no. 113475.
[9] D. Kwon and J. Yoon, "A model-based prognostic approach to predict interconnect failure using impedance analysis," *J. Mech. Sci. Technol.*, vol. 30, no. 10, pp. 4447–4452, Oct. 2016.
[10] F. X. Che and J. H. L. Pang, "Study on reliability of PQFP assembly with lead free solder joints under random vibration test," *Microelectron. Rel.*, vol. 55, no. 12, pp. 2769–2776, 2015.
[11] Y. K. Kim and D. S. Hwang, "PBGA packaging reliability assessments under random vibrations for space applications," *Microelectron. Rel.*, vol. 55, no. 1, pp. 172–179, Jan. 2015.
[12] W. Tang, B. Jing, Y. Huang, and Z. Sheng, "Feature extraction for latent fault detection and failure modes classification of board-level package under vibration loadings," *Sci. China Technol. Sci.*, vol. 58, no. 11, pp. 1905–1914, Nov. 2015.
[13] T. Wei, "Circuit board-level solder joint fatigue life model based on transfer entropy under multi-field coupling," *Sci. China*, vol. 47, no. 5, pp. 484–494, 2017.
[14] T. Wei, "Analysis method for potential failures of board-level packaging of electronic equipment PHM under vibration load," *Acta Electronica Sinica*, vol. 44, no. 4, pp. 944–951, 2016.
[15] F. Xu, C. R. Li, T. M. Jiang, and D. P. Zhang, "Fatigue life prediction for PBGA under random vibration using updated finite element models," *Exp. Techn.*, vol. 40, no. 5, pp. 1421–1435, Oct. 2016.

[16] H. Zhang, Y. Liu, J. Wang, and F. Sun, "Failure study of solder joints subjected to random vibration loading at different temperatures," *J. Mater. Sci., Mater. Electron.*, vol. 26, no. 4, pp. 2374–2379, 2015.
[17] F. Liu, "Research on degradation model of bearing capacity of corroded stay cable," *Mod. Transp. Technol.*, vol. 14, no. 3, pp. 30–34, 2017.
[18] X. Wei, J. Fang, and W. G. Wang, "Selection of sensor performance degradation model based on TOPSIS method," *Chem. Eng. Equip.*, vol. 1, pp. 5–7, Apr. 2017.
[19] J. B. Huan, D. J. Kong, and L. R. Cui, "Multi-stage correctable system degradation modeling and reliability evaluation," *J. Syst. Eng. Electron.*, vol. 38, no. 4, pp. 965–969, 2016.
[20] Z. Y. Cai, "Nonlinear accelerated degradation reliability evaluation method based on Wiener process," *Electron. Opt. Control*, vol. 2, pp. 87–90, Apr. 2016.
[21] J. Q. Liu, J. W. Xie, and H. F. Zuo, "Remaining life prediction of aero-engine based on stochastic Wiener process," *Acta Aeronautica et Astronautica Sinica*, vol. 36, no. 2, pp. 564–574, 2015.
[22] G. L. Wei and Z. J. Chen, "Prediction method of product remaining life based on multi-stage-random Wiener degradation process," *Sci. Technol. Eng.*, vol. 15, no. 26, pp. 27–34, 2015.
[23] L. T. Long, "Research on the degradation of QFP package interconnect structure based on PCMD health index," *J. Electron. Meas. Instrum.*, vol. 22, no. 228, pp. 106–114, 2019.
[24] Y. C. Zhu, "Discussion on vibration test requirements and related issues of military aircraft airborne equipment (1): GJB 150.16/16A military jet aircraft and propeller aircraft airborne equipment and external vibration test requirements and comparison analysis," *Spacecraft Environ. Eng.*, vol. 33, no. 2, pp. 127–135, 2016.
[25] Y. C. Zhu, "Discussion on vibration test requirements and related issues of military aircraft airborne equipment (2): GJB150.16/16A military helicopter and various military aircraft engine equipment vibration test requirements and comparative analysis," *Spacecraft Environ. Eng.*, vol. 3, pp. 240–246, Jun. 2016.
[26] X. J. Zhang and Z. Li, "Research on an accelerated test method based on vibration stress transformation," *Electron. Product Rel. Environ. Test.*, vol. 33, no. 1, pp. 20–23, 2015.
[27] C. Lei, D. J. Zhou, and Z. H. Wu, "Analysis of random vibration response of photoelectric interconnect PCB," *Trans. Beijing Inst. Technol.*, vol. 6, pp. 631–636, Jul. 2017.
[28] L. Zhang, "Effect of Ce on the reliability of SnAgCu solder joints of CSP36," *Chin. Rare Earths*, vol. 5, pp. 1–5, Aug. 2016.
[29] J. Y. Dong, B. Jing, Z. Sheng, F. Lu, J. Hu, and Y. Chen, "A method of board—Level solder degradation analysis under harmonic excitation using regression approximation model," in *Proc. Prognostics Syst. Health Manage. Conf. (PHM-Harbin)*, Harbin, China, Jul. 2017, pp. 1–8.
[30] J. T. Dai, L. J. Li, and Z. J. Zhang, "Analysis of warping behavior of medium and thick plates based on symplectic elastic mechanics method," *Chin. J. Solid Mech.*, vol. 36, no. 3, pp. 215–222, 2015.
[31] P. Yang, "Research on life prediction method of key components of mechanical equipment based on online monitoring information," M.S. thesis, School Mechatronics Eng., Univ. Electron. Sci. Technol. China, Chengdu, China, 2016.
[32] N. Han, "Model and prediction of remaining life based on statistical analysis," M.S. thesis, School Math. Statist., XiDian Univ., Xi'an, China, 2014.
[33] J. Feng and J. L. Zhou, "Life prediction of thermal control pump of manned spacecraft based on Wiener process," *Chin. Space Sci. Technol.*, vol. 28, no. 4, pp. 53–58, 2008.
[34] M. Li, "Research on modeling and analyzing method of degenerate failure with random inflection point," M.S. thesis, Graduate College, Nat. Univ. Defense Technol., Changsha, China, 2009.
[35] H. W. Wan, T. X. Xu, and Y. Z. He, "Application of Wiener process in nonlinear degradation modeling," *Sci. Technol. Rev.*, vol. 32, no. 2, pp. 64–67, 2014.
[36] Z. Y. Cai, "Remaining life prediction method considering random degradation and information fusion," *J. Shanghai Jiaotong Univ.*, vol. 50, no. 11, pp. 1778–1783, 2016.
[37] H. D. Zhang, "EM algorithm and its application," M.S. thesis, Zhongtai Secur. Inst. Financial Stud., ShangDong Univ., Shandong, China, 2014.
[38] Z. Y. Ca, "Bayesian method of remaining life prediction based on stochastic Wiener process," *Electron. Opt. Control*, vol. 7, pp. 93–96, Jul. 2016.
[39] T. X. Xu, H. W. Wang, and X. Zhang, "Application of EM algorithm in the estimation of hyperparameter values of random parameters in Wiener process," *Syst. Eng. Electron.*, vol. 37, no. 3, pp. 707–712, 2015.
[40] C. B. He, "Bayesian parameter estimation of Wiener process single change point model," *J. Natural Sci. Hunan Normal Univ.*, vol. 39, no. 4, pp. 84–88, 2016.
[41] J. Li, J. Bo, J. Xiaoxuan, and X. Liu, "Multi-stage degradation modeling for airborne fuel pump based on LSTAR," *J. Beijing Univ. Aeronaut. Astronaut.*, vol. 43, no. 5, pp. 880–886, 2017.

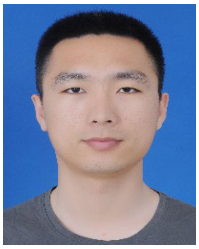

JIAYAN DONG received the B.Sc. and M.Sc. degrees from Air Force Engineering University, in 2015 and 2017, respectively. His current research interests include prognostics and health management. He is good at fault prediction, fault diagnosis, and mathematical modeling.

YINGLI LONG was born in Handan, Hebei, China. She received the B.S. degree in physics from the University of Handan, in 1990. She is the author of three books, more than ten articles, and more than ten inventions. Her research interests include basic physics teaching, physics experiment design, and reliability applications.

XIAOXUAN JIAO received the B.Sc., M.Sc., and Ph.D. degrees from Air Force Engineering University, in 2012, 2014, and 2019, respectively. He is currently a Lecturer with Air Force Engineering University. His research interests include information fusion, fault diagnosis, and prognostics.

YIFENG HUANG received the B.Sc., M.Sc., and Ph.D. degrees from Air Force Engineering University, in 2005, 2008, and 2012, respectively. He is currently an Associate Professor with Air Force Engineering University. His research interest includes the design for testability and fault diagnosis.